A Comparative Study of ULF Waves' Role in the Dynamics of Charged Particles in the Plasmasphere: Van Allen Probes Observation

Ren, Jie
Funsten, Herbert O.
Zong, Q.G.
Miyoshi, Y.
Rankin, R.
Spence, H.E.
Wygant, J. R.
Kletzing, C.A.

To be published in: Journal of Geophysical Research: Space Physics

DOI to publisher's version: 10.1029/2018JA025255

A comparative study of ULF waves' role in the dynamics of charged particles in the plasmasphere: Van Allen Probes observation

Jie Ren,[1,2] Q. G. Zong,[1] Y. Miyoshi,[2] R. Rankin,[3] H. E. Spence,[4] H. O. Funsten,[5] J. R. Wygant,[6] C. A. Kletzing,[7]

Q.-G.Zong, Institute of Space Physics and Applied Technologies, Peking University, Beijing 100871, China. (qgzong@pku.edu.cn)

[1]Institute of Space Physics and Applied Technology, Peking University, Beijing, China

[2]Solar-Terrestrial Environmental Laboratory, Nagoya University, Nagoya, Japan

[3]Department of Physics, University of Alberta, Edmonton, Alberta, Cananda

[4]Department of Physics Institute for Earth, Oceans and Space, University of New Hampshire, Durham, New Hampshire, USA

This article has been accepted for publication and undergone full peer review but has not been through the copyediting, typesetting, pagination and proofreading process, which may lead to differences between this version and the Version of Record. Please cite this article as doi: 10.1029/2018JA025255

Abstract. By analyzing observations from Van Allen Probes in its inbound and outbound orbits, we present evidence of coherent enhancement of cold plasmaspheric electrons and ions due to drift-bounce resonance with ULF waves. From 18:00 UT on 28 May 2017 to 10:00 UT on 29 May 2017, newly formed poloidal mode standing ULF waves with significant electric field oscillations were observed in two consecutive orbits when Probe B was travelling inbound. In contrast to observations during outbound orbits, the cold (< 150 eV) electorns measured by the HOPE instrument were characterized by flux enhancements several times larger and bi-directional pitch angle distributions during inbound orbits. The electron number density inferred from upper hybrid waves is twice as larger as during inbound orbits, which were also confirmed by an increase of spacecraft potential. The observed ULF waves are identified as second harmonic modes that satisfy the drift-bounce resonant condition of N=1 with cold electrons. An enhancement of the plas-

[5]Los Alamos National Laboratory, Los Alamos, USA

[6]School of Physics and Astronomy, University of Minnesota, Twin Cities, Minneapolis, Minnesota, USA

[7]Department of Physics and Astronomy, University of Iowa, Iowa City, Iowa, USA

maspheric ion number density to restore charge neutrality of plasmas in inbound orbits is observed, which is associated with an increase of ULF wave periods. The observations suggest that the dynamics of plasmaspheric electrons is modified by ULF waves through drift-bounce resonance, and that plasmaspheric ions are indirectly impacted.

1. Introduction

The plasmasphere is filled with low temperature (a few eV) electrons and ions of ionospheric origin, and highly dominated by the superposition of the convection and corotation electric fields under different geomagnetic activities [*Darrouzet et al.*, 2009; *Singh et al.*, 2011; *Lemaire et al.*, 2005]. The dynamic processes of the plasmasphere consist of its erosion or inward motion that occurs within a few hours in response to the increasing geomagnetic activities [e.g. *Spasojević et al.*, 2004; *Goldstein and Sandel*, 2005; *Gallagher and Adrian*, 2007], and its refilling that occurs over a period of a few days after a geomagnetic storm [e.g. *Sandel and Denton*, 2007; *Reinisch et al.*, 2009]. The plasmasphere contains various density structures including large-scale (plumes and notches), medium-scale (shoulders, channels, fingers, and crenulations) and small-scale features (irregularities), which usually unfold in the time scales from minutes to hours [*Darrouzet et al.*, 2009].

The well-known resonant condition for poloidal mode ULF wave-particle interactions is $\omega - m\omega_d = N\omega_b$, where ω and m are the wave frequency and azimuthal wave number, respectively, ω_d and ω_b are the frequencies of particle's drift and bounce motions, respectively, and N is an integer indicating the number of wavelengths through which particles pass in the azimuthal direction within one bounce period. Aside from plasmasphere, the inner magnetosphere also contains the radiation belts and ring current regions. Outer radiation belt electrons can be effectively accelerated by ULF waves through drift resonance (N=0), in which the bounce frequency far exceeds the drift frequency and wave frequency [*Zong et al.*, 2009; *Mann et al.*, 2013; *Foster et al.*, 2015; *Zhou et al.*, 2015; *Kabin et al.*, 2007]. Drift resonant electrons stay in the accelerating wave electric field when their drift

velocity matches the wave propagation velocity in the azimuthal direction. Increasingly, spacecraft observations reveal that the dynamics of ring current oxygen ions can be significantly affected by ULF waves through drift-bounce resonance ($N = 0, \pm1, \pm2, \ldots$) [*Zong et al.*, 2012, 2017a; *Ren et al.*, 2016, 2017a; *Yang et al.*, 2011]. ULF waves have mainly been used to estimate the plamsapshere ion mass density based on the eigenfrequencies of standing Alfvén waves [*Poulter et al.*, 1984; *Vellante et al.*, 2014a; *Takahashi et al.*, 2006; *Darrouzet et al.*, 2006]. Some recent spacecraft observations suggest that ULF waves also play an important role in the acceleration of the cold plasmaspheric electrons through drift-bounce resonance (N≠0) [*Ren et al.*, 2017b; *Zong et al.*, 2017b].

In the event of *Ren et al.* [2017b], cold electrons (< 200 eV) show flux enhancement and bi-directional pitch angle distributions (Figure 1e) when there are ULF waves present (Figure 1b) as observed by Probe B during consecutive outbound and inbound orbits (Figure 1a). It is noteworthy that the electron number density (Figure 1f) was enhanced during the wave-particle interaction from 0100-0400 UT, while it is not very clear in the next orbit (0900-1300 UT). Therefore, it is hard to judge whether the observed enhancement of the electron number density is related to ULF wave-particle interaction or spatial structures.

Ren et al. [2017b] compared the cold electron observations from HOPE instrument on different orbits of the Van Allen Probes that have orbital periods of about 9 h near the equatorial plane [*Mauk et al.*, 2013]. By taking advantage of different observations made over outbound and inbound orbits of the Van Allen Probes, the present study explores the role of ULF waves in the dynamics of cold plasmaspheric electrons measured by the HOPE instrument, and colder electrons (out of the HOPE instrument measurement range)

inferred from upper hybrid waves and/or spacecraft potentials, as well as plasmaspheric ions.

2. Observation

2.1. Overview

Figure 2 gives an overview of RBSP-B measurements between 18:00 UT on 28 May 2017 and 10:00 UT on 29 May 2017. During this time interval, Probe B travelled outbound and inbound through the plasmasphere twice, as shown in Figure 2a, where the apogee of each orbit is marked by a blue star. Figure 2b -2d show the electron energy spectrum and pitch angle distributions for 150 eV<W< 1 keV and W < 150 eV measured by the HOPE instrument [*Funsten et al.*, 2013], respectively. In contrast to observations made during outbound orbits (Part I and Part III), cold (< 150 eV) electrons show obvious flux enhancement, while the associated pitch angle distributions show a bi-directional dispersion feature during inbound orbits (Part II and Part IV). In contrast, the electron flux in the energy range from 150 eV to 1 keV is decreased in Part II and Part IV. The upper hybrid resonance line marked by the white line in Figure 2e can be used to determine the electron number density (Figure 2f) from the upper hybrid wave dispersion relation [*Kurth et al.*, 2015; *Ren et al.*, 2017b]. The electron number density is roughly doubled in Part II and Part IV, which is further confirmed by the increase of spacecraft potential in Figure 2g. Figure 2h and 2j show the wavelet power spectra of the original B_y and E_z components, respectively. The B_y and E_z components, after subtracting a 10 min running average, are shown in Figure 2i and 2k, respectively. In Part I-II, there are strong magnetic field oscillations but weak electric field oscillations in the Pc4 range when Probe B is near the magnetic equator (Mlat$\sim$0). But in Part III-IV, magnetic and electric

field oscillations become weaker and stronger, respectively, when Probe B is located in the southern hemisphere (Mlat∼-16°). The ULF wave observations are thus consistent with properties of a second harmonic mode, which has an electric field antinode and a magnetic field node at the magnetic equator [*Southwood and Kivelson*, 1982; *Dai et al.*, 2013]. The ULF wave periods in Part II and Part IV are higher than those in Part I and Part III. Figure 2l presents the wavelet power spectrum of the B_y component observed by GOES 15 at geosynchronous orbit on the dayside (MLT$\simeq$ 12-14) during the Part I-II time interval, and in the nightside sector (MLT $\simeq$19-23) during the Part III-IV time interval. The ULF waves observed by GOES 15 during the time interval of Part I and Part IV occurred during the recovery phase of a magnetic storm, as indicated by the SYM-H index in Figure 2m. There were a also series of substorm activities indicated by the AL index in Figure 2n.

In order to eliminate the possibility that the electron density enhancements in Part II and IV result from satellite encountering a stable and localized density structure, joint observations from Probe A and B are shown in Figure 4. The first two panels present that Probe B leads Probe A by about 4 hours. The evolution of electron density profile observed by Probe A and B is denoted by upper hybrid wave resonance lines (Figure 4c and 4e) and spacecraft potentials (Figure 4d and 4f). The electron density enhancements observed by Probe B are marked by the red rectangular bars on the top and red shadow regions in Figure 4f. The density enhancements were not observed in the former orbit during 12:00-20:00 UT on 28 May 2017 for Probe A and 08:00-16:00 UT on 28 May 2017 for Probe B, which means the density enhancements in Part II and IV are irrelevant to a pre-existing density structure. During the orbit of Probe A among Part II and Part

IV, the asymmetry of density profile did not appear when ULF waves were observed by Probe A travelling outbound and inbound, which is marked by the black shadow region in Figure 4d. These joint observations demonstrate that the electron density enhancements observed by Probe B are related to ULF waves when drift-bounce resonance occurs.

2.2. Wave properties and their interaction with cold electrons

In order to explore whether the enhancement of the cold electron flux and electron number density is related to wave-particle interaction, the wave properties of the poloidal mode (B_r and E_a) are analyzed over a shorter time scale in Figure 3. The ULF waves in the Part I-IV time interval are identified as second harmonic mode oscillations. Additionally, the following properties are identified, (1) according to wavelet coherence analysis in Figure 3g and 3h, E_a leads B_r by 90° in Part II when Mlat > 0, and E_a lags B_r by 90° in Part III and IV when Mlat < 0 [*Singer et al.*, 1982; *Le et al.*, 2017; *Ren et al.*, 2017b]; (2) the observed ULF wave frequency is consistent with the eigenfrequency of the second harmonic mode indicated by the red line in Figure 3i and 3j, which is estimated from the dipole magnetic field models used in [*Degeling et al.*, 2010; *Ren et al.*, 2016, 2017a]. In this calculation, the Pedersen conductance of the ionosphere boundary is infinite and the density model obeys a power-law distribution with an index of 4.0 [*Cummings et al.*, 1969]. The equatorial number density is inferred from the upper hybrid dispersion relation with particles assumed to be protons. Considering the affect by the stretched magnetosphere under the solar wind impact, another model by *Rankin et al.* [2000] is used to estimate the eigenfrequencies of the fundamental mode (dashed magenta lines in Figure 3i-3j). The results are basically consistent with the calculations by the former model, which means the affect by the stretched magnetosphere in the inner magnetosphere can be

ignored in the modeling calculation. One requirement of drift-bounce resonance theory is that the poloidal mode should be standing waves with adequate electric field oscillations. According to the observations in Figure 3c-3h, this requirement is satisfied in Part II-IV but not Part I. Therefore, as shown in Figure 3k and 3l, cold electrons in the Part II-IV time interval show higher flux and bi-directional pitch angle distribution features. The electron number density in Part III is half that in Part II and Part IV. Probe A, lagging Probe B by about 4 hours, observed cold electrons with bi-directional pitch angle distributions similar to Part II-IV, but the electron number density was at the same level as Part I and Part III (not shown here). These observations imply that the electron number density is rapidly enhanced after the occurrence of drift-bounce resonance (observed in Part II and Part IV), and then gradually restored to its initial level (observed in Part III and by Probe A) due to radial diffusion or other dynamic processes.

The averaged electron spectra in Part I and Part II are given in Figure 5a, as indicated by the black and red lines, respectively. In Part I, the electrons in the energy range from 15 eV to 150 eV show a power law distribution, which implies there is no wave-particle interaction when the wave electric field is small [*Ren et al.*, 2016, 2017b]. These cold electrons are accelerated in Part II through N=1 drift-bounce resonance with second harmonic mode ULF waves [*Ren et al.*, 2017b]. The red shaded region in Figure 5a represents the resonant energy range estimated from the B_r wave bandwidth in Part II [*Ren et al.*, 2017b]. It implies that colder ($\sim$ eV) electrons out of the HOPE instrument measurement range are also affected by ULF waves. In Figure 5b, the electron spectra (15-150 eV) in Part III and Part IV deviate significantly from a power law distribution, which is consistent with the observations shown in Figure 3i. These findings suggest that the acceleration of

cold electrons in Part III-IV are also a consequence of drift-bounce resonance with second harmonic poloidal mode waves. In Figure 5b, the estimated resonant energy range in Part III (grey shaded region) is higher than that in Part IV (red shaded region) due to the lower wave periods in Part III, which indicates that $\sim$ eV electrons in Part III may not be accelerated by ULF waves. This probably explains why the electron number density in Part III is similar to that in Part I, and lower than in Part II and IV. Unlike the cold (15-150 eV) electrons in Part II and Part IV, the electron flux in the range of 150 eV-1 keV is significantly decreased, which is presumably related to ULF waves based on the comparative analysis. However, it is an open question whether the electron flux decrease in the range of 150 eV-1 keV is related to drift-bounce resonance because these energies are far from the resonant energy indicated by the shaded regions in Figure 5, and their pitch angle distributions do not show bi-directional dispersion features.

3. Discussion and Summary

The comparison of Van Allen Probes observations during outbound and inbound orbits provides new sights into the dynamics of the plamsmasphere as it responds to ULF waves and drift-bounce resonance. During the event in this study, there is no strong solar wind impact on the magnetosphere, which is characterized by low speed ($\sim$ 350 km/s) solar wind, continuously positive values of IMF B_z, as well as stable SYM-H index. There are intense substorm activities before the appearance of ULF waves in Part I and Part IV. During such substorm activities, ULF waves are known to be excited by outer and inner magnetosphere sources[*Keiling and Takahashi*, 2011], as shown in Figure 6. Fast mode waves excited by outer magnetosphere sources such as bursty bulk flows propagate across geomagnetic field lines into the inner magnetosphere [*Kepko et al.*, 2001; *Hsu and*

McPherron, 2007; *Keiling and Takahashi*, 2011]. These fast mode ULF waves will couple with the local Alfvén waves and excite transverse standing waves through field line resonance at locations where fast mode frequencies match the eigenfrequencies of magnetic field lines [*Kivelson et al.*, 1984; *Zong et al.*, 2009; *Degeling et al.*, 2007]. On the other hand, substorm-injected energetic ions will drift westward in the inner magnetosphere and provide free energy for second harmonic transverse standing Alfvén waves excited through the drift-bounce resonant instability [*Chisham and Orr*, 1991; *Glassmeier et al.*, 1999; *Ren et al.*, 2017b]. Figure 2f shows that second harmonic mode ULF waves exist in the plasmasphere boundary layer, which is outside the plasmapause that can be regarded as an internal turning point for ULF waves [*Walker*, 2005; *Zhu and Kivelson*, 1989; *Lee*, 1996]. According to CRRES observations, "classic" step-like plasmapauses are detected in a minority (16%) of plasmapause crossings, whereas the outer boundary of the plasmasphere has complex and variable density structures in most cases [*Moldwin et al.*, 2002]. Previous studies have revealed that standing ULF waves can be excited in the plasmasphere boundary layer [*Liu et al.*, 2013; *Ren et al.*, 2015; *Zong et al.*, 2009]. There is also a large-scale plume structure in the pre-midnight and afternoon MLT sectors, which extends beyond the main plasmapause into the outer magnetosphere [*Moldwin et al.*, 2004; *Darrouzet et al.*, 2006]. The plume structure can impact dayside magnetic reconnection when it extends to the magnetopause [*Walsh et al.*, 2014]. Cold electrons in the structured boundary of the plasmasphere (e.g. plasmasphere boundary layer or plumes) can be accelerated through drift-bounce resonance (N$\neq$0) with excited ULF waves, and then diffused radially. In order to restore plasma charge neutrality, the ion mass/number density must increase, which is evidenced by an increase of wave periods in Part II and Part IV.

Combined with the work by *Ren et al.* [2017b] , this paper has revealed the role of ULF waves in the dynamics of plasmasphere including acceleration of cold plasmaspheric electrons and modification of electron and ion density profiles through drift-bounce resonance using Van Allen Probe observations.

Figure 6 indicates that ULF waves are limited to the duskside and have a certain extent of radial distribution. Utilizing multi-spacecraft observations in different regions of magnetosphere, *Ren et al.* [2017b] also found that ULF waves interacting with cold electrons are mainly confined to the duskside sector up to L∼8. *Hao et al.* [2017] inferred the existence of localised ULF waves within a density structure on the duskside plasmasphere (e.g. plumes) through analysis of "boomerang-shaped" relativistic electron pitch angle distributions on the dawnside. *Degeling et al.* [2018] investigated how evolutions of ULF wave distributions can be controlled by the development of plasmaspheric plume structure using a 3-D MHD model. The present study suggests 1. A large portion of the plasmasphere on the duskside can be affected by ULF waves through drift-bounce resonance; 2. The spatial distribution of ULF waves should be taken into consideration in assessing the affect of wave-particle interactions on the dynamics of inner magnetosphere plasma. Combined with the remote-sensing approach based on ground station observations [*Piersanti et al.*, 2017; *Vellante et al.*, 2014b], in-situ multi-spacecraft observations will promote our understanding of ULF waves' affect on the spatial scales and temporal evolutions of the dynamics of plasmasphere. In previous studies, the principle use of ULF waves was to estimate the plasma mass density as a diagnostic [*Allan and Poulter*, 1992; *Darrouzet et al.*, 2009]. The role of ULF waves in affecting the evolutions of structure in

the plasmasphere has not been considered extensively [*Darrouzet et al.*, 2009; *Singh et al.*, 2011], and is deserving of more attention in the future.

Acknowledgments. This work was supported by the National Natural Science Foundation of China (41421003 and 41627805). R. Rankin acknowledges the financial support from NSERC and the Canadian Space Agency. Processing and analysis of the HOPE data was supported by the Energetic Particle, Composition, and Thermal Plasma (RBSP-ECT) investigation funded under NASAs Prime contract no. NAS5-01072. All RBSP-ECT data are publicly available at the Web site http://www.RBSP-ect.lanl.gov/. We acknowledge NASA CDAWeb (http://cdaweb.gsfc.nasa.gov/) for providing all data in this article.

References

Allan, W., and E. Poulter, ULF waves-their relationship to the structure of the Earth's magnetosphere, *Reports on Progress in Physics*, *55*(5), 533, 1992.

Chisham, G., and D. Orr, Statistical studies of giant pulsations (Pgs): harmonic mode, *Planet. Space Sci.*, *39*(7), 999–1006, 1991.

Cummings, W., R. O'sullivan, and P. Coleman, Standing Alfvén waves in the magnetosphere, *J. Geophys. Res.*, *74*(3), 778–793, doi:10.1029/JA074i003p00778, 1969.

Dai, L., et al., Excitation of poloidal standing Alfvén waves through drift resonance wave-particle interaction, *Geophys. Res. Lett.*, *40*(16), 4127–4132, doi:10.1002/grl.50800, 2013.

Darrouzet, F., J. de Keyser, and V. Pierrard, *The Earth's Plasmasphere: A CLUSTER and IMAGE Perspective*, Springer, 2009.

Darrouzet, F., et al., Analysis of plasmaspheric plumes: Cluster and image observations, *Ann. Geophys.*, *24*(6), 1737–1758, 2006.

Degeling, A., R. Rankin, K. Kabin, R. Marchand, and I. Mann, The effect of ulf compressional modes and field line resonances on relativistic electron dynamics, *Planet. Space Sci.*, *55*(6), 731–742, 2007.

Degeling, A., R. Rankin, K. Kabin, I. Rae, and F. Fenrich, Modeling ULF waves in a compressed dipole magnetic field, *J. Geophys. Res.*, *115*(A10), 2010.

Degeling, A., I. Rae, C. Watt, Q. Shi, R. Rankin, and Q.-G. Zong, Control of ULF Wave Accessibility to the Inner Magnetosphere by the Convection of Plasma Density, *J. Geophys. Res.*, *123*, doi:10.1002/2017JA024874, 2018.

Foster, J., J. Wygant, M. Hudson, A. Boyd, D. Baker, P. Erickson, and H. E. Spence, Shock-induced prompt relativistic electron acceleration in the inner magnetosphere, *J. Geophys. Res.*, *120*(3), 1661–1674, doi:10.1002/2014JA020642, 2015.

Funsten, H., et al., Helium, Oxygen, Proton, and Electron (HOPE) mass spectrometer for the radiation belt storm probes mission, *Space Sci. Rev.*, *179*(1-4), 423–484, doi:10.1007/s11,214–013–9968–7, 2013.

Gallagher, D., and M. L. Adrian, Two-dimensional drift velocities from the image EUV plasmaspheric imager, *J.Atmos.Sol.CTerr.Phys.*, *69*(3), 341–350, 2007.

Glassmeier, K.-H., S. Buchert, U. Motschmann, A. Korth, and A. Pedersen, Concerning the generation of geomagnetic giant pulsations by drift-bounce resonance ring current instabilities, *Ann. Geophys.*, *17*(3), 338–350, 1999.

Goldstein, J., and B. Sandel, The global pattern of evolution of plasmaspheric drainage plumes, *Inner Magnetosphere Interactions: New Perspectives from Imaging. Geophysi-*

cal Monograph Series, vol.159, pp. 1–22, 2005.

Hao, Y., et al., Relativistic electron dynamics produced by azimuthally localized poloidal mode ULF waves: Boomerang-shaped pitch angle evolutions, *Geophys. Res. Lett.*, *44*(15), 7618–7627, 2017.

Hsu, T.-S., and R. McPherron, A statistical study of the relation of pi 2 and plasma flows in the tail, *J. Geophys. Res.*, *112*(A5), 2007.

Kabin, K., R. Rankin, I. R. Mann, A. W. Degeling, and R. Marchand, Polarization properties of standing shear Alféen waves in non-axisymmetric background magnetic fieldss, *Ann. Geophys.*, *25*(3), 815–822, 2007.

Keiling, A., and K. Takahashi, Review of Pi2 models, *Space Sci. Rev.*, *161*, 63–148, 2011.

Kepko, L., M. Kivelson, and K. Yumoto, Flow bursts, braking, and Pi2 pulsations, *J. Geophys. Res.*, *106*(A2), 1903–1915, 2001.

Kivelson, M. G., J. Etcheto, and J. G. Trotignon, Global compressional oscillations of the terrestrial magnetosphere: The evidence and a model, *J. Geophys. Res.*, *89*(A11), 9851–9856, 1984.

Kurth, W., S. De Pascuale, J. Faden, C. Kletzing, G. Hospodarsky, S. Thaller, and J. Wygant, Electron densities inferred from plasma wave spectra obtained by the waves instrument on van allen probes, *J. Geophys. Res.*, *120*(2), 904–914, 2015.

Le, G., et al., Global observations of magnetospheric high-m poloidal waves during the 22 june 2015 magnetic storm, *Geophys. Res. Lett.*, *44*(8), 3456–3464, 2017.

Lee, D.-H., Dynamics of mhd wave propagation in the low-latitude magnetosphere, *J. Geophys. Res.*, *101*(A7), 15,371–15,386, 1996.

Lemaire, J. F., K. I. Gringauz, D. L. Carpenter, and V. Bassolo, *The Earth's plasmasphere*, Cambridge University Press, 2005.

Liu, W., et al., Poloidal ULF wave observed in the plasmasphere boundary layer, *J. Geophys. Res.*, *118*(7), 4298–4307, 2013.

Mann, I. R., et al., Discovery of the action of a geophysical synchrotron in the Earths van allen radiation belts, *Nature communications*, *4*, doi:doi:10.1038/ncomms3795, 2013.

Mauk, B., N. J. Fox, S. Kanekal, R. Kessel, D. Sibeck, and A. Ukhorskiy, Science objectives and rationale for the radiation belt storm probes mission, *Space Sci. Rev.*, *179*(1-4), 3–27, doi:10.1007/s11,214–012–9908–y, 2013.

Moldwin, M., J. Howard, J. Sanny, J. Bocchicchio, H. Rassoul, and R. Anderson, Plasmaspheric plumes: Crres observations of enhanced density beyond the plasmapause, *J. Geophys. Res.*, *109*(A5), 2004.

Moldwin, M. B., L. Downward, H. Rassoul, R. Amin, and R. Anderson, A new model of the location of the plasmapause: CRRES results, *J. Geophys. Res.*, *107*(A11), 2002.

Piersanti, M., et al., Comprehensive Analysis of the Geoeffective Solar Event of 21 June 2015: Effects on the Magnetosphere, Plasmasphere, and Ionosphere Systems, *Solar Physics*, *292*(11), 169, doi:10.1007/s11207-017-1186-0, 2017.

Poulter, E., W. Allan, J. Keys, and E. Nielsen, Plasmatrough ion mass densities determined from ULF pulsation eigenperiods, *Planet. Space Sci.*, *32*(9), 1069–1078, 1984.

Reinisch, B. W., M. B. Moldwin, R. E. Denton, D. L. Gallagher, H. Matsui, V. Pierrard, and J. Tu, Augmented empirical models of plasmaspheric density and electric field using image and cluster data, in *The Earths Plasmasphere*, pp. 231–261, 2009.

Rankin, R., F. Fenrich, and V. T. Tikhonchuk, Shear Alfvén waves on stretched magnetic field lines near midnight in Earth's magnetosphere, *Geophys. Res. Lett.*, *27*(20), 3265–3268, doi:10.1029/2000GL000029, 2000.

Ren, J., Q. G. Zong, Y. F. Wang, and X. Z. Zhou, The interaction between ULF waves and thermal plasma ions at the plasmaspheric boundary layer during substorm activity, *J. Geophys. Res.*, *120*(2), 1133–1143, doi:10.1002/2014JA020766, 2015.

Ren, J., Q. G. Zong, X. Z. Zhou, R. Rankin, and Y. F. Wang, Interaction of ULF waves with different ion species: pitch angle and phase space density implications, *J. Geophys. Res.*, *121*(10), 9459–9472, doi:10.1002/2016JA022995, 2016.

Ren, J., Q. G. Zong, X. Z. Zhou, R. Rankin, Y. F. Wang, S. J. Gu, and Y. F. Zhu, Phase relationship between ULF waves and drift-bounce resonant ions: a statistical study, *J. Geophys. Res.*, *122*(7), 7087–1096, doi:10.1002/2016JA023848, 2017a.

Ren, J., et al., Low-energy (< 200 ev) electron acceleration by ULF waves in the plasmaspheric boundary layer: Van allen probes observation, *J. Geophys. Res.*, doi: 10.1002/2017JA024316, 2017b.

Sandel, B. R., and M. H. Denton, Global view of refilling of the plasmasphere, *Geophys. Res. Lett.*, *34*(17), 2007.

Singer, H. J., W. J. Hughes, and C. T. Russell, Standing Hydromagnetic Waves Observed by ISEE 1 and 2: Radial Extent and Harmonic, *J. Geophys. Res.*, *87*, 3519–3529, doi: 10.1029/JA087iA05p03519, 1982.

Singh, A., R. Singh, and D. Siingh, State studies of Earth's plasmasphere: A review, *Planet. Space Sci.*, *59*(9), 810–834, 2011.

Southwood, D. J., and M. G. Kivelson, Charged particle behavior in low-frequency geomagnetic pulsations. ii - graphical approach, *J. Geophys. Res.*, *87*, 1707–1710, 1982.

Spasojević, M., H. Frey, M. Thomsen, S. Fuselier, S. Gary, B. Sandel, and U. Inan, The link between a detached subauroral proton arc and a plasmaspheric plume, *Geophys. Res. Lett.*, *31*(4), 2004.

Takahashi, K., P. J. Chi, R. E. Denton, and R. L. Lysak, Magnetospheric ULF waves: Synthesis and new directions. geophysical monograph 169, in *Magnetospheric ULF Waves: Synthesis and New Directions*, vol. 169, 2006.

Vellante, M., M. Piersanti, and E. Pietropaolo, Comparison of equatorial plasma mass densities deduced from field line resonances observed at ground for dipole and IGRF models, *J. Geophys. Res.*, *119*(4), 2623–2633, doi:10.1002/2013JA019568, 2014a.

Vellante, M., M. Piersanti, B. Heilig, J. Reda, and A. Del Corpo, *Magnetospheric plasma density inferred from field line resonances: Effects of using different magnetic field models*, 1–4 pp., 2014b.

Walker, A., Excitation of field line resonances by sources outside the magnetosphere, *Ann. Geophys.*, *23*(10), 3375–3388, 2005.

Walsh, B., J. Foster, P. Erickson, and D. Sibeck, Simultaneous ground-and space-based observations of the plasmaspheric plume and reconnection, *Science*, *343*(6175), 1122–1125, 2014.

Yang, B., et al., Pitch angle evolutions of oxygen ions driven by storm time ulf poloidal standing waves, *J. Geophys. Res.*, *116*, doi:A03207, doi:10.1029/2010JA016047, 2011.

Zhou, X.-Z., et al., Imprints of impulse-excited hydromagnetic waves on electrons in the van allen radiation belts, *Geophys. Res. Lett.*, *42*(15), 6199–6204, doi:

10.1002/2015GL064988, 2015.

Zhu, X., and M. G. Kivelson, Global mode ULF pulsations in a magnetosphere with a nonmonotonic alfvén velocity profile, *J. Geophys. Res.*, *94*(A2), 1479–1485, 1989.

Zong, Q.-G., Y. F. Wang, H. Zhang, S. Y. Fu, H. Zhang, C. R. Wang, C. J. Yuan, and I. Vogiatzis, Fast acceleration of inner magnetospheric hydrogen and oxygen ions by shock induced ULF waves, *J. Geophys. Res.*, *117*, A11,206, doi:10.1029/2012JA018,024, 2012.

Zong, Q.-G., R. Rankin, and X. Z. Zhou, The interaction of ultra-low-frequency Pc3-5 waves with charged particles in earths magnetosphere, *Reviews of Modern Plasma Physics*, *1*(1), 10, 2017a.

Zong, Q.-G., Y. F. Wang, J. Ren, X. Z. Zhou, S. Y. Fu, R. Rankin, and H. Zhang, Corotating drift-bounce resonance of plasmaspheric electron with poloidal ULF waves, *Earth and Planetary Physics*, *1*, 2–12, doi:10.26464/epp2017002, 2017b.

Zong, Q.-G., et al., Energetic electrons response to ULF waves induced by interplanetary shocks in the outer radiation belt, *J. Geophys. Res.*, *114*, A10,204, doi:10.1029/2009JA014,393, 2009.

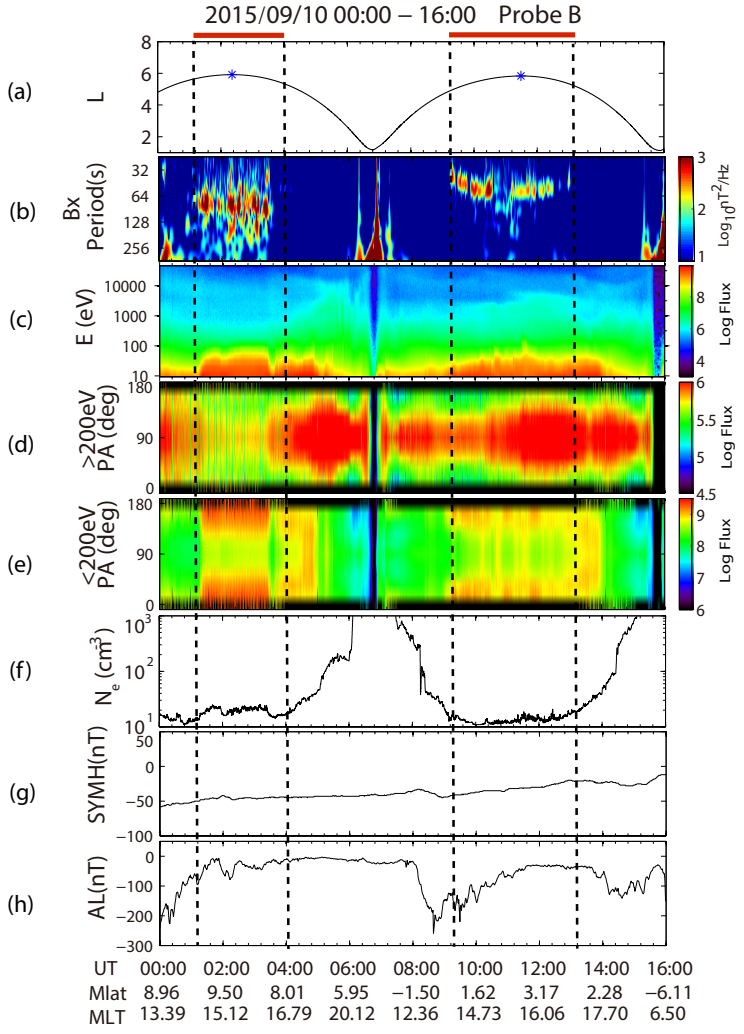

Figure 1. Observation of the magnetic field and electrons by Van Allen Probe B and ground magnetic index during 00:00-16:00 UT on 10 September 2015. (Based on *Ren et al.* [2017b]). (a) L shell of Van Allen Probe B with apogees marked by blue star signs. (b) Wavelet power spectrum of B_x component in GSE coordinates. (c-e) Electron energy spectrum, pitch angle distributions with E>200 eV and E<200 eV, respectively. (f) Electron number density inferred from the detected upper-hybrid resonance line from Probe B/EMFISIS. (g) SYM-H index. (f) AL index. The red rectangular bars on the top and the black vertical dashed lines illustrate the time intervals when there are ULF wave-particle interactions in two consecutive orbits. Magnetic latitude (Mlat) and magnetic local time (MLT) are labelled at the bottom.

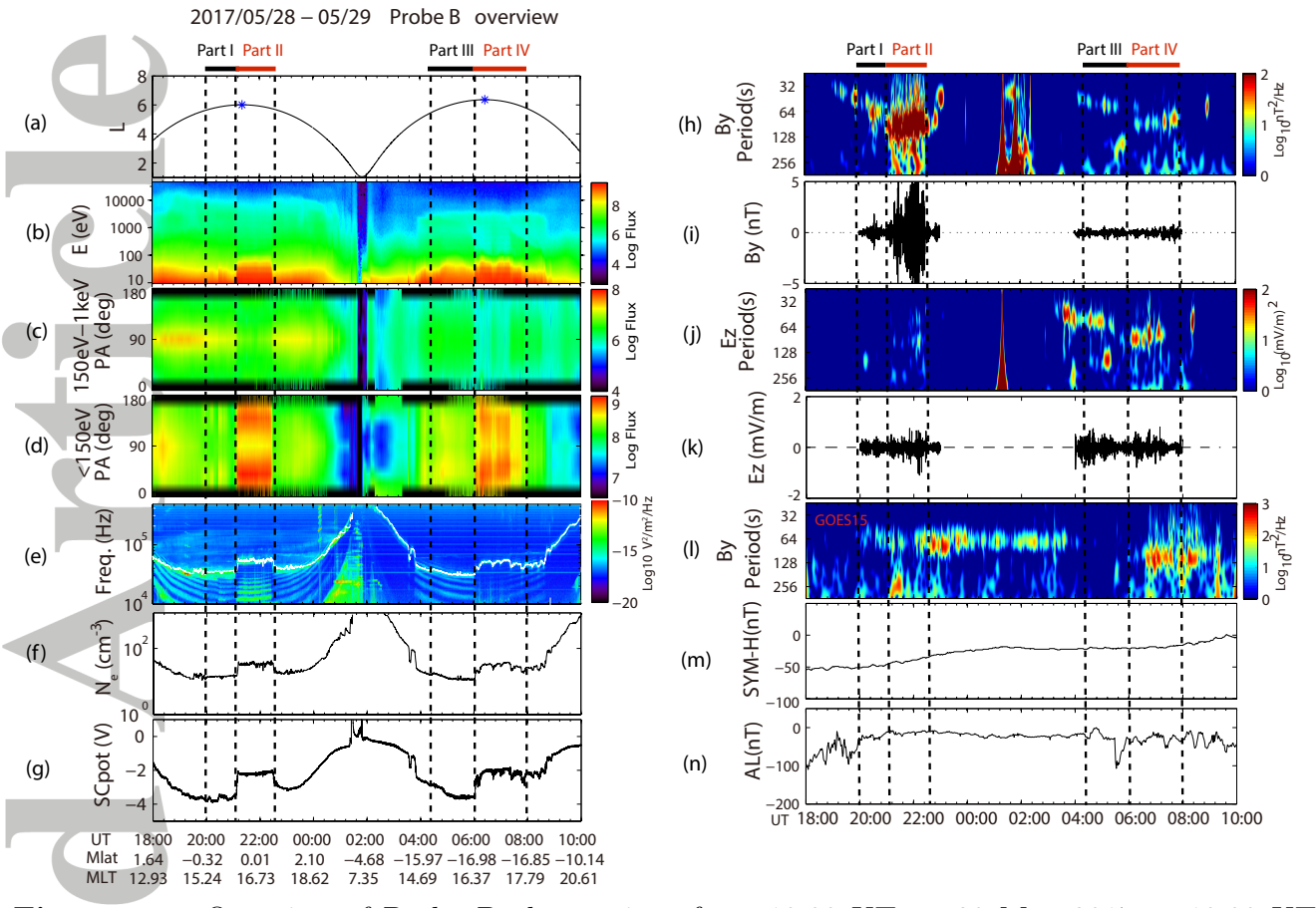

Figure 2. Overview of Probe B observations from 18:00 UT on 28 May 2017 to 10:00 UT on 29 May 2017. (a) L shell. (b-d) Electron energy spectrum, pitch angle distributions with 150 eV<W<1 keV and W<150keV, respectively. (e) Frequency-time spectrum of electric field spectral intensity from Probe B/EMFISIS with the upper hybrid resonance line marked by the white line. (f) Electron number density inferred from the upper hybrid resonance line. (g) Spacecraft potential. (h) Wavelet power spectrum of original B_x component in GSE coordinates. (i) B_y after substracting the 10 min running average. (j) Wavelet power spectrum of original E_z. (k) E_z after substracting the 10 min running average. (l) Wavelet power spectrum of original B_y from GOES 15 spacecraft. (m) SYM-H index. (n) AL index. The red rectangular bars on the top illustrate the time intervals (Part II and Part IV) when there are ULF wave-particle interactions, and the black represent the time intervals (Part I and Part III) of the control groups.

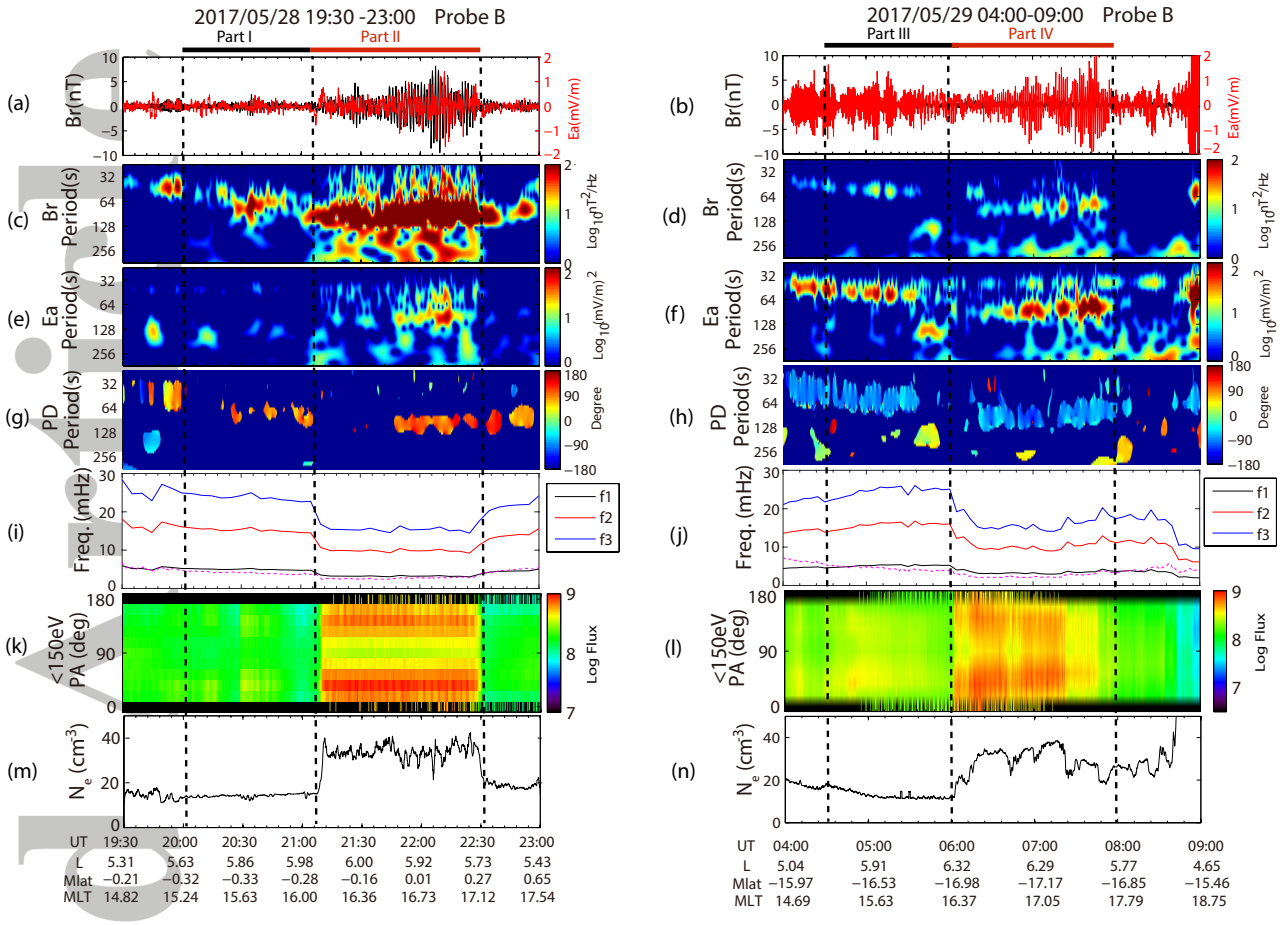

Figure 3. Wave properties of the poloidal ULF waves and electron observations from Probe B during 19:30-23:00 UT on 28 May 2017 and 04:00-09:00 UT on 29 May 2017. (a and b) Radial magnetic field component (B_r) and azimuthal electric field (E_a) of poloidal mode ULF waves; (c-f) Wavelet power spectra of B_r and E_a; (g and h) Phase difference between B_r and E_a, where the positive value means that E_a leads B_r in the wave phase, and the negative value means in opposite; (i and j) Eigenfrequencies of fundamental (f_1), second harmonic (f_2), and third harmonic (f_3) modes from modeling calculation assuming that the geomagnetic field is dipole. The dashed magenta lines indicate the eigenfrequencies of fundamental mode by taking into account the affect by the stretched magnetosphere; (k and i) Pitch angle distributions of electrons with W< 150 eV; (m and n) Electron number density.

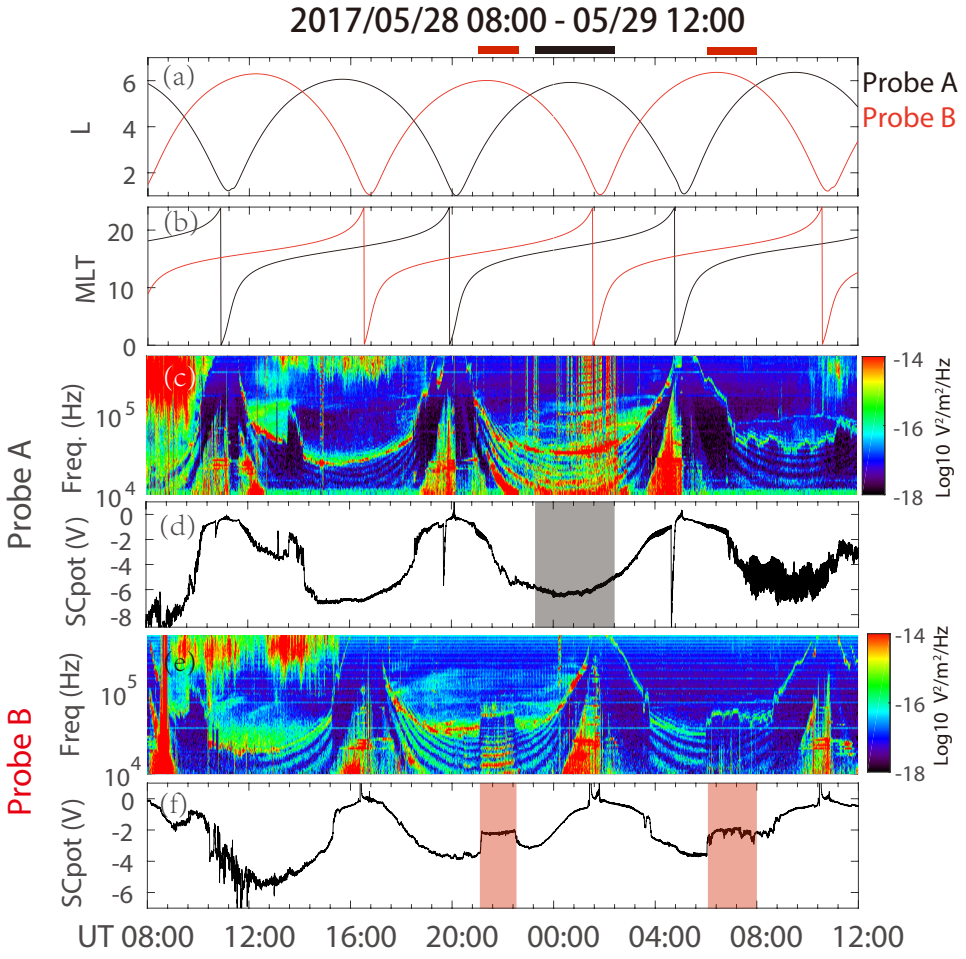

Figure 4. Joint observations from Probe A and B. (a) L shell value; (b) Magnetic local time (MLT); (c) and (e) Frequency-time spectrum of electric field spectral intensity for Probe A and B, respectively; (d) and (f) Spacecraft potential for Probe A and B, respectively. The red rectangular bars on the top correspond to Part II and IV, which are further marked by red shadow regions in panel f. The black rectangular bar indicates the time interval when ULF waves were observed by Probe A, which is further marked by black shadow regions in panel d.

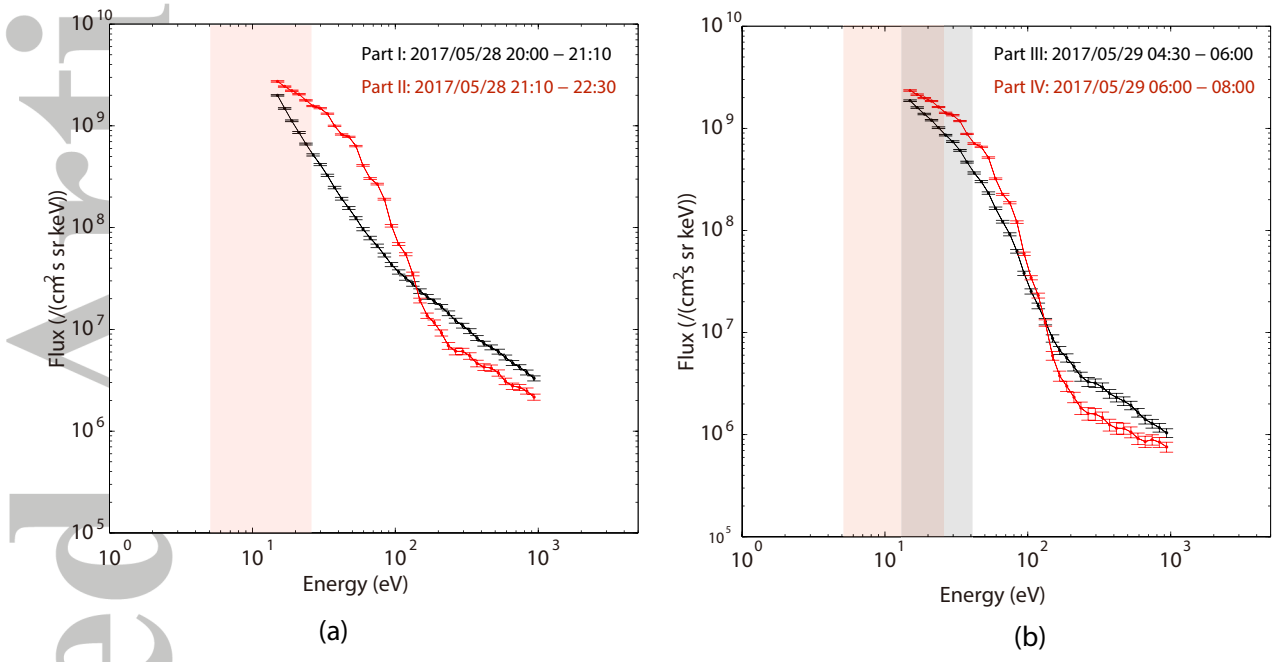

Figure 5. (a) The averaged electron spectra of Part II (red line) and its control group-Part I (black line); the red shaded region indicates the resonant energy range corresponding to the B_r wave bandwidth defined as wavelet power dropping from the maximum to its half in Part II. (b) The averaged electron spectra of Part IV (red line) and its contrast groupPart III (black line); the red and gray shaded regions represent the resonant energy ranges corresponding to the B_r wave bandwidth in Part IV and Part III, respectively.

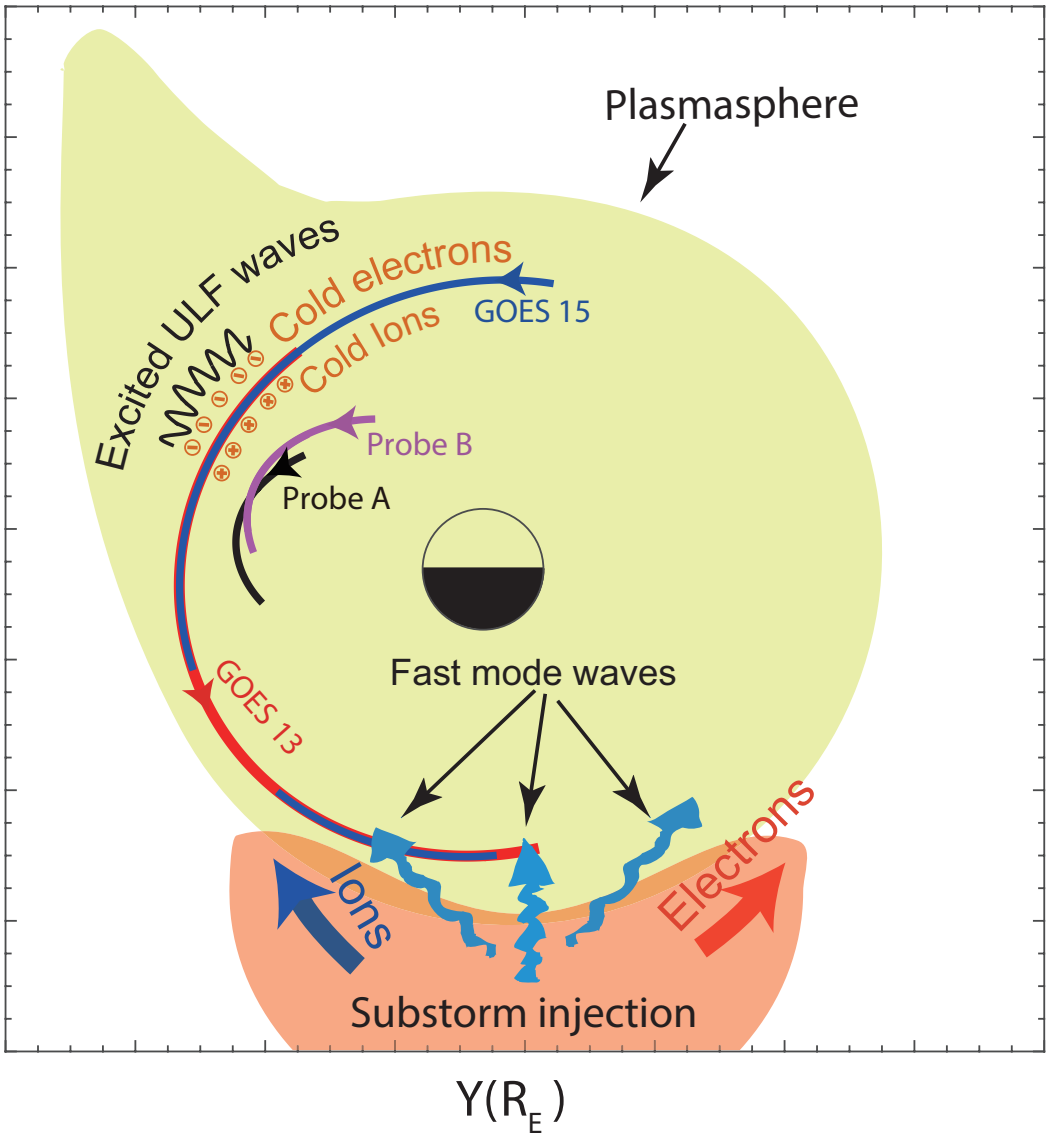

Figure 6. A schematic showing of the possible dynamic process in this study. The orbits of several spacecraft where ULF waves can be observed are marked in this schematic. During substorm activities, the transverse Alfvén waves can be excited by the internal sources: the injected ions drifting westward through drift-bounce resonant instability or by the external source: the fast mode waves through the field line resonance. The cold plasmaspheric electrons will be affected by the excited standing ULF waves through the drift-bonce resonance. To restore the charge neutrality, plasmaspheric ion number density also will be enhanced to the same level as the plasmaspheric electrons in the wave-particle interacting region.